IS-T 1750

Physical Metallurgy and Properties of TiNiSn and PtMnSb

by

Zhong, Bo

MS Thesis submitted to Iowa State University

Ames Laboratory, U.S. DOE
Iowa State University
Ames, Iowa 50011

Date Transmitted: January 10, 1997

PREPARED FOR THE U.S. DEPARTMENT OF ENERGY
UNDER CONTRACT NO. W-7405-Eng-82.

DISCLAIMER

TABLE OF CONTENTS

LIST OF TABLES

LIST OF FIGURES

ABSTRACT

The single crystals of TiNiSn and polycrystalline PtMnSb were grown by the flux and melt cooling method. Their lattice parameters and structures were determined by x-ray diffraction. The effect of impurities on the growth of TiNiSn single crystals was investigated. It was found that the concentration of chlorine plays a key role in determining the chemical composition of the phases that are formed.

The heat capacity and magnetic susceptibility of TiNiSn was measured in a temperature range from 4.7 K to room temperature. Magnetic measurements show that the TiNiSn is paramagnetic, and that it does not order magnetically.

CHAPTER I

INTRODUCTION

Both TiNiSn and PtMnSb are intermetallic compounds which have the MgAgAs structure. This structure can be thought of as consisting of four interpenetrating cubic fcc sublattices (Fig. 1), A(0, 0, 0); B(1/4, 1/4, 1/4); C(1/2, 1/2, 1/2) and D(3/4, 3/4, 3/4), one of which, set C, is empty.

The physical properties of compounds with an ordered lattice of vacancies have been intensively studied in recent years. de Groot et al.[1] showed that this specific feature may lead to an occurrence of a new class of materials - the so-called semimetallic ferromagnetics. The loss of the inversion symmetry at Mn positions and a strong interaction of the valence electrons with the magnetic sublattice can produce the full spin polarization of d-electrons at the Fermi level in the ferromagnetic state of PtMnSb [1,2]. Studies of the magneto-optical properties on this material have shown that a polycrystal of PtMnSb has a Kerr rotation angle of 1.86 degree at room temperature [3]. The

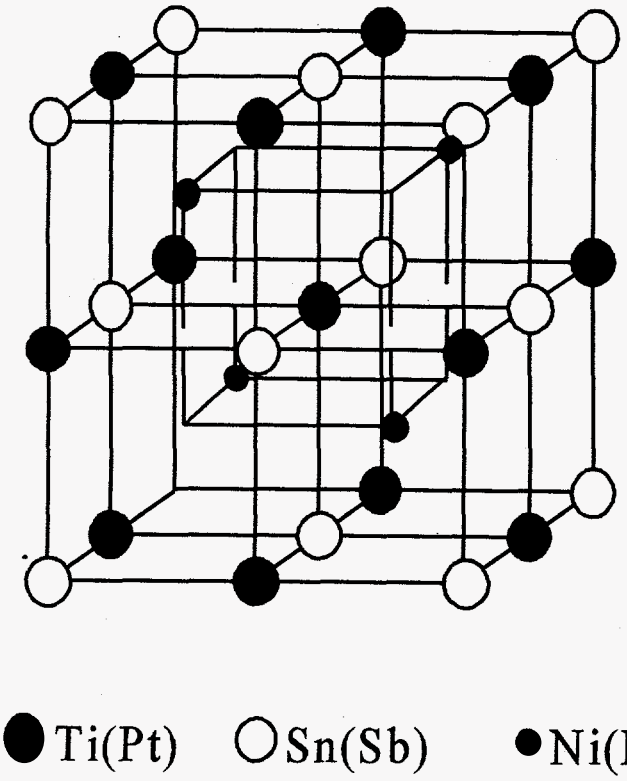

Figure 1. The crystal structure of TiNiSn and PtMnSb.

nonmagnetic intermetallic compound TiNiSn, with the structure of MgAgAs, has a narrow 0.1-0.2eV gap near the Fermi level [4,5].

The susceptibility of TiNiSn was measured by Skolozdra, et al. from 78 to 300 °C [6] which was reported in Chemical Abstracts. But since there is no complete English version of their article, their results cannot be compared with our work.

In order to further investigate the properties of TiNiSn, we had to grow single crystals in the laboratory. The preparation methods of TiNiSn crystal could be found in many articles [4,5,7,8]. All of these authors used an arc melting method. In our studies, we used a flux growth method to obtain large TiNiSn crystals. The advantage of the flux growth technique is that it is easy to separate the product from the flux and ordinarily these crystals are of a higher purity and lower strain than polycrystalline samples. The purpose of growing PtMnSb was to try to find a better method to grow large single crystals of this material.

The thesis is organized as follows: Chapter II discusses the flux growth method. The preparation of the sample and temperature profile for growing TiNiSn and PtMnSb

crystals are given in this chapter. Chapter III is concerned with the effect of impurities, in particular chlorine, on the single crystal structure of the TiNiSn. In Chapter IV we describe the heat capacity of TiNiSn, while Chapter V deals with the susceptibility of TiNiSn. Summary and conclusions make up Chapter VI. Some experimental data are presented in the Appendix.

CHAPTER II

CRYSTAL GROWTH AND STRUCTURE DETERMINATION

A. Growth of TiNiSn

The TiNiSn samples used in this investigation were prepared in Ames Laboratory. The same flux growth method as that used by P. C. Canfield and Z. Fisk [9] was used to prepare TiNiSn single crystals. The raw materials used in synthesizing the TiNiSn compound are almost all over 99.9 at. % pure. Two different kinds of titanium starting metals were used in our investigation, one was titanium crystal bar and the other titanium sponge. Both of the titanium raw materials have similar purities labeled by the manufacturers but because of the different impurity levels different products were synthesized. This unusual behavior will be discussed later. The results of chemical analyses of titanium crystal bar are listed in the table I.

In the growth of TiNiSn compound, we used Sn as the flux material. Ti, Ni and Sn were weighed in a atomic ratio (TiNi to Sn) of 9 : 91. These elements were put into a 2ml or 5ml crucible and sealed in a quartz tube under a vacuum

Table I Chemical Analysis of Ti Crystal Bar (ppm atomic)

Impurity*	Concentration
Mn	35
Fe	4
V	4
Al	7
Cr	30
Ni	2
Zr	3
O	300
C	27
N	16

* Elements not listed may be present at a concentration level of < 2 ppm atomic.

of ~10^{-4} torr. In order to separate the flux and the synthesized crystals, a certain amount of quartz wool acting as a filter was put on top of the crucible. Each sample weighed about 7 grams. The sealed samples were put into a resistance furnace and heated to 1150 °C and held at that temperature for 3 hours in order to melt and evenly mix the solutes in the solvent. Then the ampule-crucible assemblage was cooled to a temperature 600 °C at a cooling rate of 5.5 °C/hour. During the cooling process, TiNiSn crystals nucleated and grew. Finally, The assembled crucible was put into a centrifuge to separate the crystals from the flux at 600 °C. The synthesis process is described by Figure 2. After separating the samples from the flux by centrifuging ("spin-out") they were allowed to cool down to room temperature in air.

It should be noted that the upper temperature was limited to 1150 °C because the softening temperature for quartz is about 1200 °C, and a higher temperature may result in the collapse of the quartz tube.

When Ti-cystal bar was used as a starting material, the resultant TiNiSn crystals have a pyramid shape with a size of 3 ~ 4 mm.

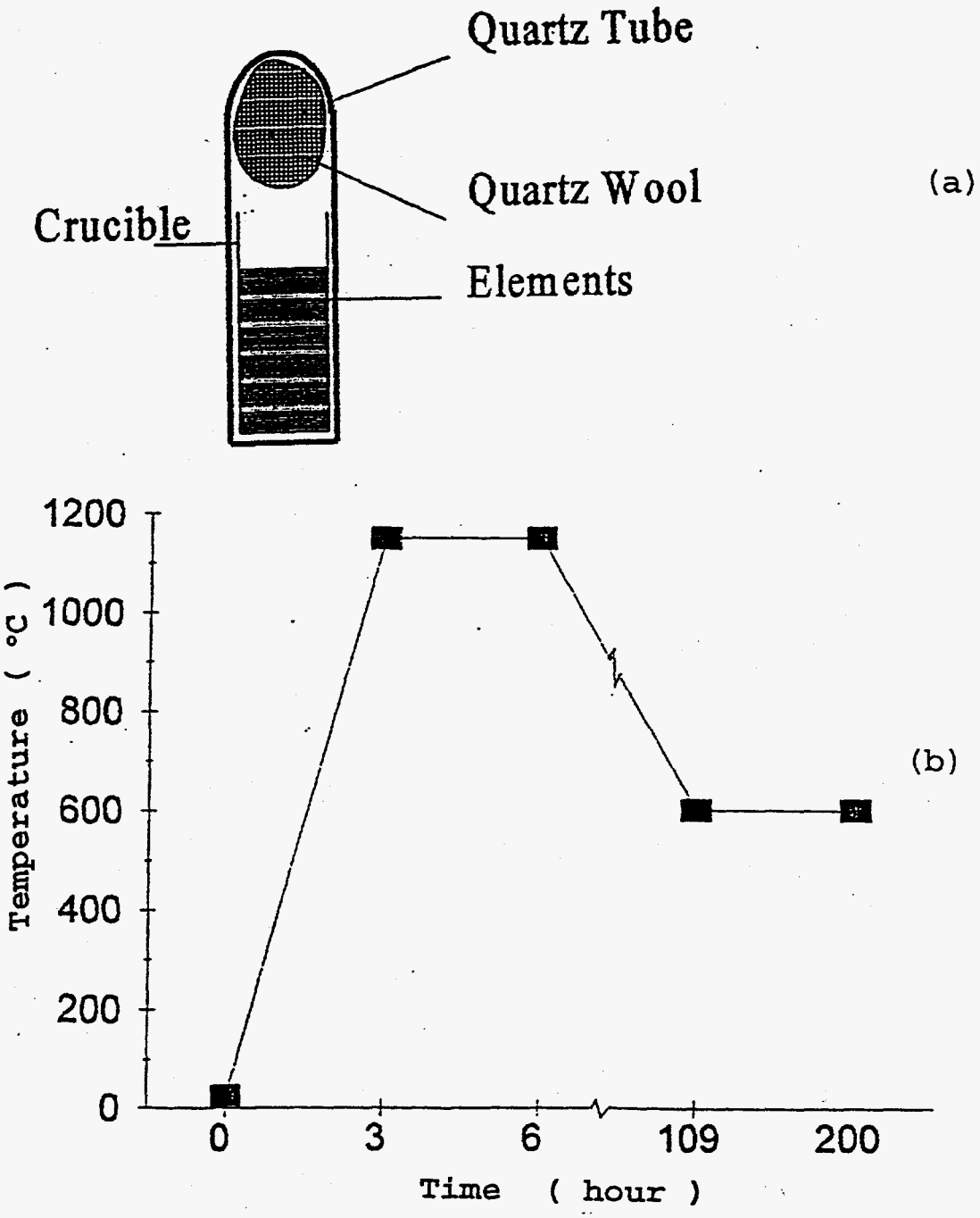

Figure 2. (a) Crucible assembly and (b) temperature profile for the growth of TiNiSn.

B. Growth of PtMnSb

Bulk PtMnSb samples were grown using a slightly different method than that used to grow of TiNiSn single crystals. In this case, no flux was used. Instead the sample was grown slow cooling of a stoichiometric melt, ie. The ratio of the platinum, manganese and antimony in this process is 1:1:1. The temperature profile is shown in Figure 3b. The highest temperature again was limited by the softening point of the quartz, and the final annealing temperature by the phase relationships in the corresponding binary phases of the three elements. At the beginning of the growth progress, the furnace temperature was slowly increased to 1150 °C and kept at this temperature for 3 hours so that the reactants could react. Then the temperature was lowered in a rate of 2.67 °C/hr to 750 °C and kept at the temperature 750 °C for 50 hours, the power cut off, and let the furnace cooled down naturally. The sealed tube was then taken out.

This technique yielded large, dense, polycrystalline ingots, and is essentially a Bridgeman growth with poorly controlled nucleation.

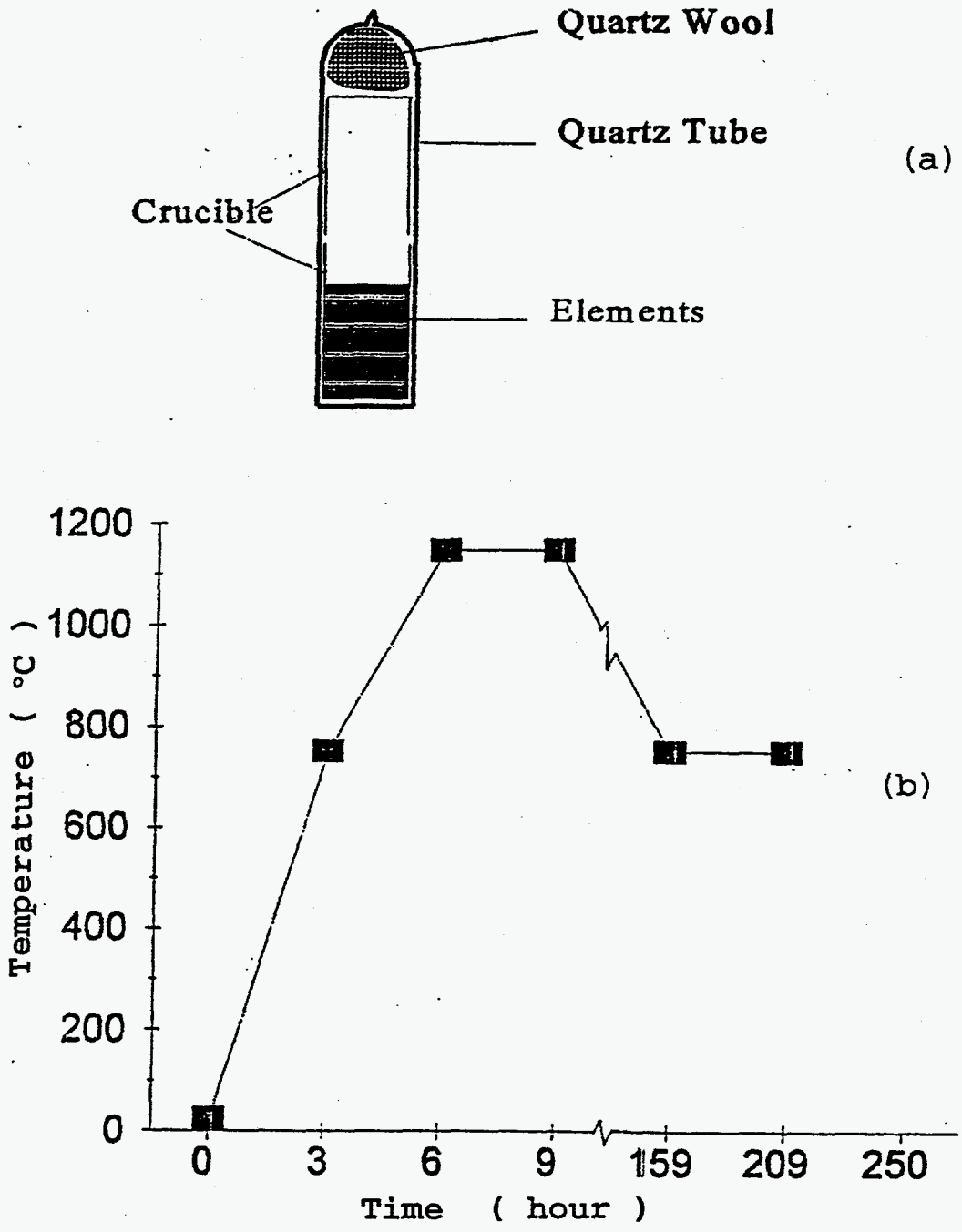

Figure 3. (a) Crucible assembly and (b) temperature profile for the growth of TiNiSn.

C. Determination of the lattice parameters

X-ray diffraction patterns were taken on a SCINTAG diffractometer using a powder sample. The X-ray diffraction pattern for TiNiSn is shown in Figure 4. Copper K_α radiation (1.5406 Å)was used for examining both TiNiSn and PtMnSb.

Several factors effect the accurate determination of the lattice constants. These factors include misalignment of the instrument, use of a flat specimen, absorption in the specimen, displacement of the specimen from the diffractometer axis and divergence of the incident beam. To determine lattice parameters of TiNiSn and PtMnSb, a least-square method was used.

According to the theory of a least-square refinement, the equation of a line in two dimensional space is:

$$Y = mX + b \qquad (1)$$

If we have two error-free pair of values for X and Y for measurements which are related by this equation, we can obtain a unique answer for the constants m and b.

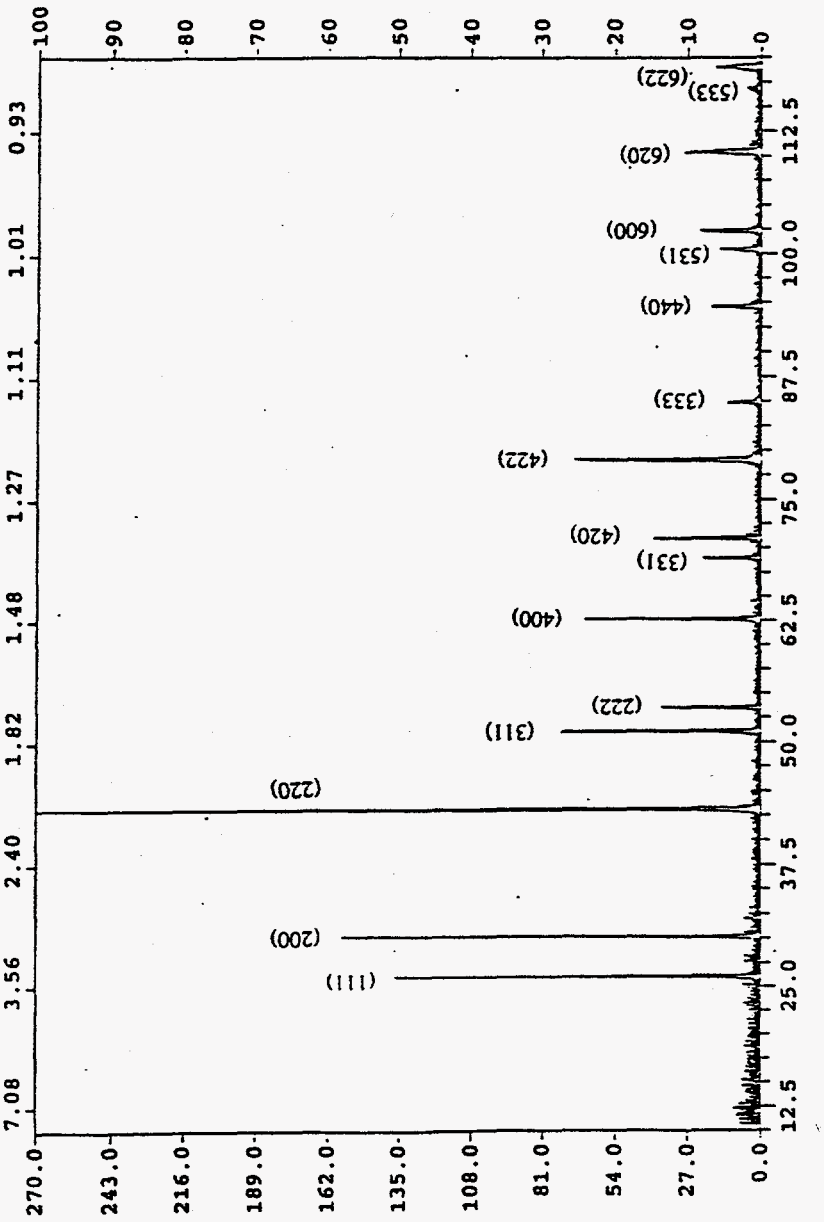

Figure 4. X-ray pattern of TiNiSn.

Sometimes, we have several pairs of values which contain random errors, and we need to obtain those values of m and b that best fit the set of observations.

Often the errors in X are negligible compared with those in Y, and a better choice of m and b would result with less error by having the difference between Y and mX + b. We let m_o and b_o be the best estimate of m and b. Then, the error in the ith observation is:

$$\Delta_i = m_o X_i + b_o - Y_i \qquad (2)$$

The least-square method states that the best fit parameters are those for which the sum of the errors for all observation is a minimum.

To minimize above equation, we partially differentiate with respect to m_o and b_o , and in turn, we equate the derivatives to zero. Hence,

$$m_o \sum_i^N X_i^2 + b_o \sum_i^N X_i = \sum_i^N X_i Y_i \qquad (3)$$

$$m_o \sum_i X_i + b_o = \sum_i Y_i \qquad (4)$$

which constitute a pair of simultaneous equations, easily

solved for m_o and b_o.

For the lattice parameter of a substance, we use the Bragg equation:

$$2d\sin\theta = \lambda . \qquad (5)$$

where θ is the angle of diffraction, and λ is the wavelength of the x-ray beam and for the cubic system, d is given by

$$d = \frac{a}{\sqrt{h^2+k^2+l^2}} \qquad (6)$$

In equation (6), a is the lattice parameter and h, k, and l are the indices of that plane hkl which gives rise to the diffracted peak. From this equation, we can derive a error equation:

$$\frac{\Delta d}{d} = \frac{\Delta a}{a} . \qquad (7)$$

For a diffractometer, the displacement of the specimen from the diffractometer axis is usually the largest single source of error. It causes an error given by

$$\frac{\Delta d}{d} = -\frac{D}{R}\frac{\cos^2\theta}{\sin\theta} \qquad (8)$$

where D is the specimen displacement parallel to the reflecting-plane normal [10].

Combining equations (7) and (8) and noting that $\Delta a=a-a_o$ we have

$$a = a_o - a_o \frac{D}{R}\frac{\cos^2\theta}{\sin\theta}. \qquad (9)$$

or writing this equation in another form we obtain

$$a = a_o + K\frac{\cos^2\theta}{\sin\theta}. \qquad (10)$$

where $K=-a_oD/R$ is a constant. This is a linear equation and we use $\cos^2\theta/\sin\theta$ as the argument. The interception of this line on ***a*** axis is the "error-free" lattice parameter of the tested cubic crystal.

Two methods can be used with above equation. The first one is to plot the experimental values on a graph of ***a*** vs $\cos^2\theta/\sin\theta$, get a straight line and extrapolate that line to ***a*** axis and find out the lattice parameter. The second one is to use the least square method. In this thesis I used the least square method to obtain the lattice parameters for TiNiSn and PtMnSb.

The graph of ***a*** as a function of $\cos^2\theta/\sin\theta$ for the x-

ray pattern of TiNiSn shown in Figure 4 is given in Figure 5. From the best fit straight line, we have derived the lattice parameter ***a***.

The average value of the lattice parameter, ***a***, for the TiNiSn, determined from the X-ray diffraction data is 5.930Å. Generally the higher the diffraction angle, the more accurate the lattice parameter. The largest diffraction peak is 622, its corresponding lattice parameter is 5.930 Å. The value obtained from linear regression method is 5.931Å. The reported values from the references [7,8] are 5.937Å and 5.941Å.

The average value of the lattice parameter ***a*** for PtMnSb is 6.190Å, while that from the linear regression is 6.199Å. The X-ray diffraction pattern and the graph of the linear fit are shown in Figure 6 and Figure 7, respectively.

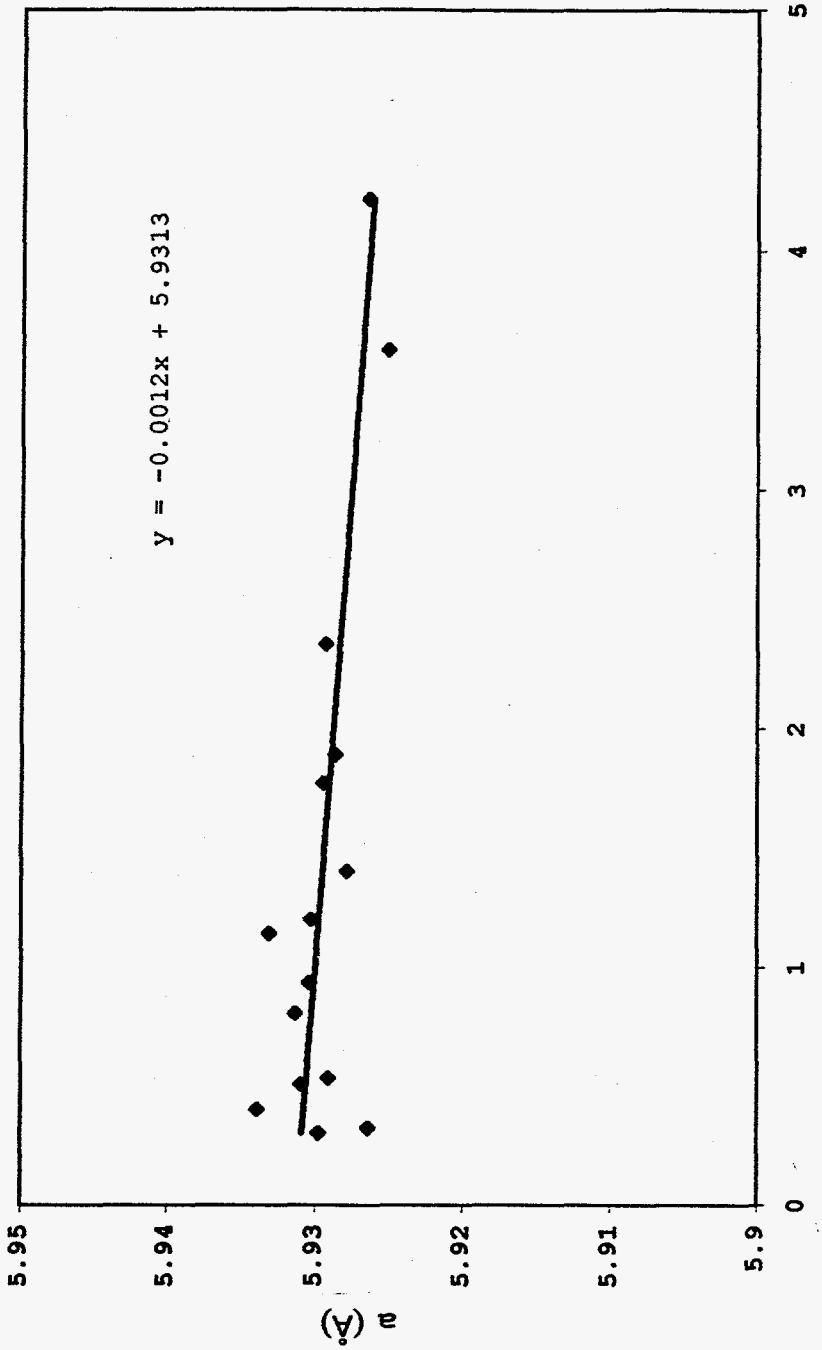

Figure 5. Linear regression of the experimental data for TiNiSn.

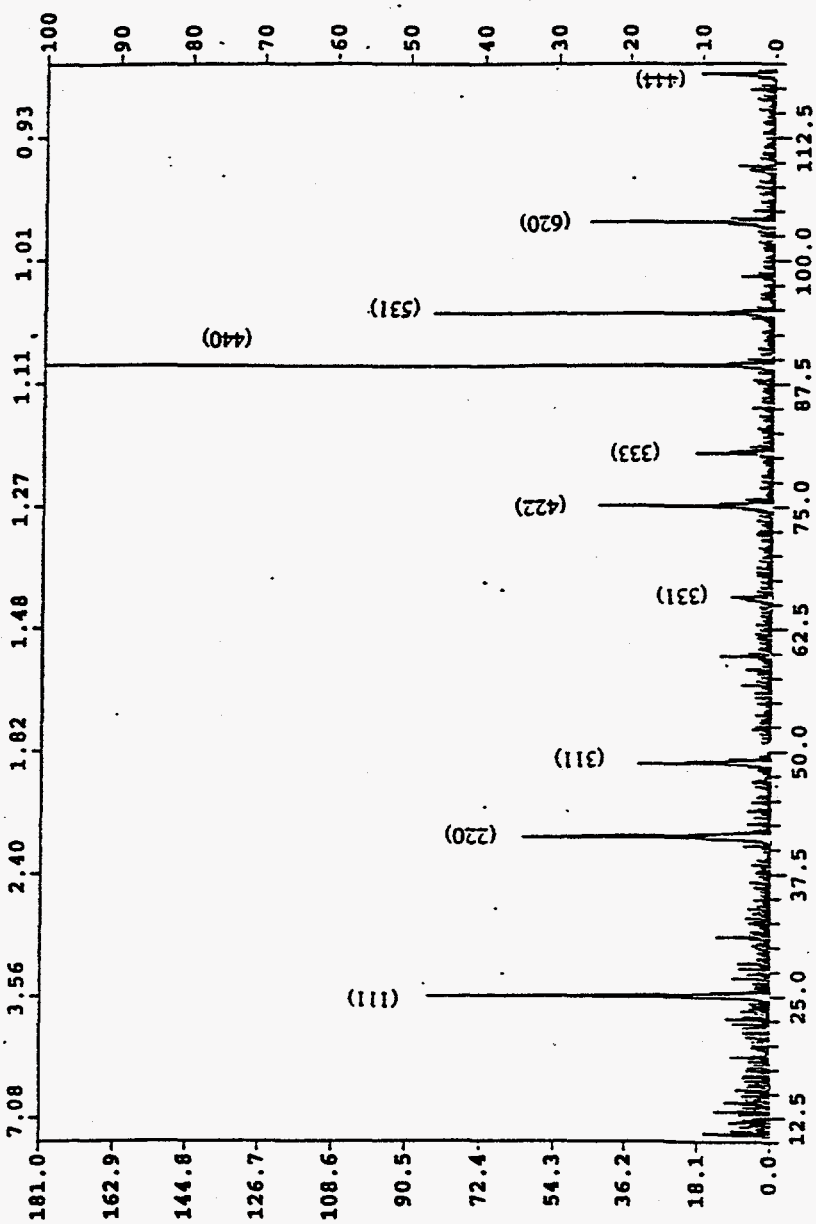

Figure 6. X-ray pattern of PtMnSb.

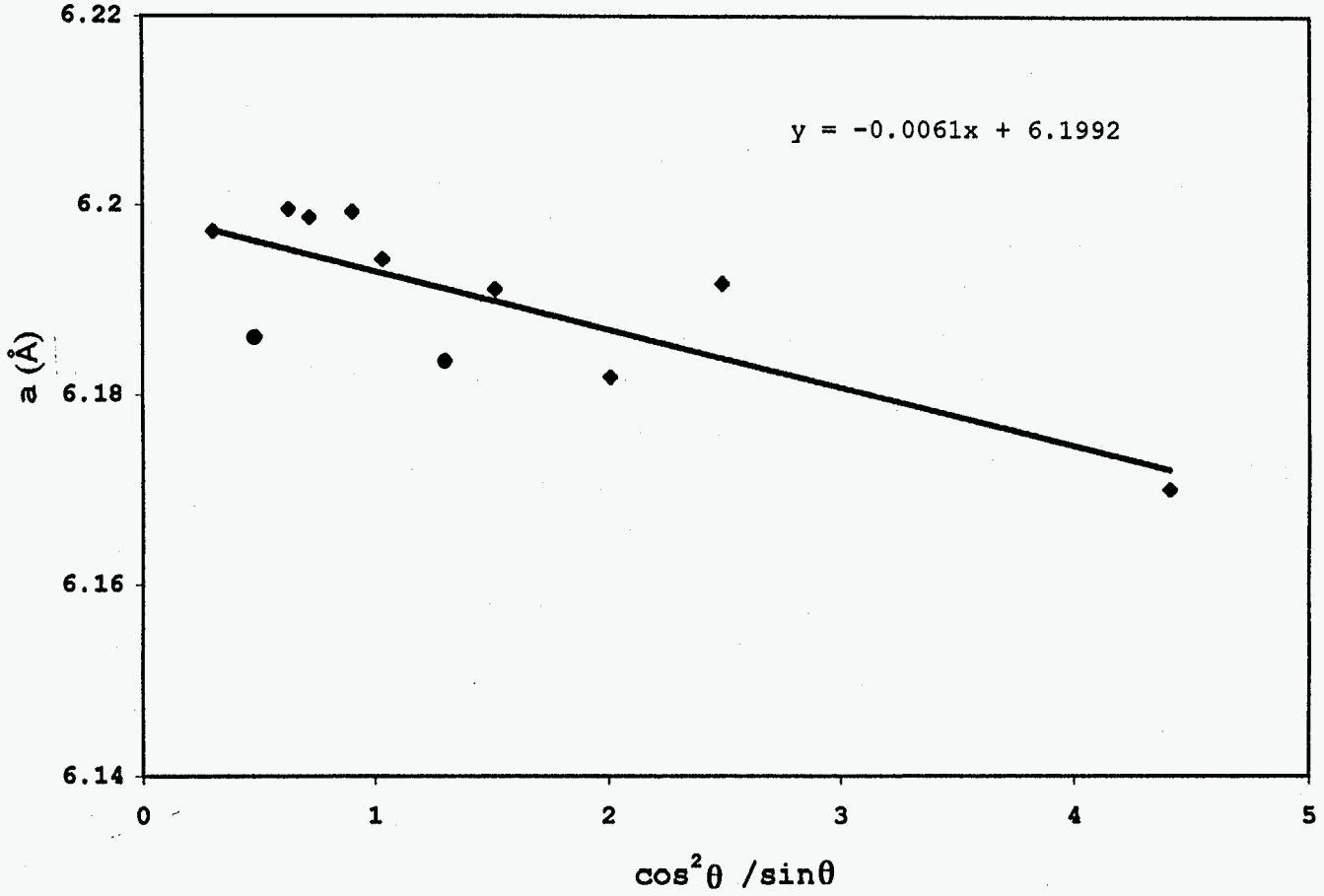

Figure 7. Linear regression of the experimental data for PtMnSb.

CHAPTER III

The Effect of Impurities on Phase Stability

In growing TiNiSn single crystals, two kinds of titanium feed-stock were used: one is titanium crystal bar and the other is titanium sponge. Even though they had almost the same purity (see Tables I - VI), we found a very interesting phenomenon. That is we obtained two kinds of crystals: one with a pyramid shape and the other with a flat plate shape. The former was grown using crystal bar titanium. The latter was found in samples when the titanium sponge was used. X-ray analyses showed the pyramid phases to be TiNiSn and the two dimensional phase to be Ni_3Sn_4. This indicated some thing, probably an impurity, changed the mechanism which controlled the crystal growth process and affected the obtained phases. The question is: which impurity(ies) may have influenced the crystal growth process?

Impurities which might interfere with the crystal growth, such as iron, copper, silicon, carbon, chromium and oxygen were added to the starting Ti(crystal bar) + Ni + Sn

composition at the hundreds to thousands ppm atomic level. After a series growths, we found that these impurities had no strong effects on the formation of crystals.

By carefully checking the crucibles used in our growths studies, we found that many small crystals formed on the wall of the crucible. After the spin-out, the quartz tubes showed a deep dark color, especially for samples in which sponge titanium was the starting material. This suggested that a volatile impurity existed in the sponge titanium material. To test this hypothesis sponge titanium was arc-melted before preparing another round of crystals. With the arc-melted sponge titanium, the crystals had the pyramid shape and X-rays confirmed that the TiNiSn structure was obtained. The various titanium samples were analyzed by Auger and laser mass atomic spectrometry. The results are listed in Table II to VI.

Auger analyses were made on four different areas of the sponge titanium starting material and the arc-melted titanium. A problem with Auger analysis is it only gives information about the surface area down to 100 Å and there can be a big change of a constituent, on the sample surface compared to the interior.

Table II Auger Analysis Before Sputtering

Element	Concentration (%)			
	Area 1	Area 2	Area 3	Area 4
C	4.96	18.33	15.86	1.67
O	4.93	17.36	17.06	15.53
F	2.75	3.70	1.81	3.55
Cl	0.44	0.68	0.48	0.93
Na	9.58	10.44	4.36	3.54
S	1.10	0.79	0.92	1.28
Ti	76.23	48.69	59.51	73.50

Table III Auger Analysis After Sputtering

Element	Concentration (%)			
	Area 1	Area 2	Area 3	Area 4
C	10.12	10.88	11.70	14.57
O	7.97	16.51	4.70	10.56
F	1.08	1.05	1.72	1.27
Cl	0.12	1.63	0.06	0.45
Na	5.25	4.78	3.65	4.93
S	0.71	0.75	0.76	0.37
Ti	74.75	64.39	77.39	67.85

Table IV Auger Analysis of Arc-melted Sponge Titanium

Element	Concentration (%)		
	Area 1	Area 2	Area 3
C	40.12	39.78	22.73
O	12.26	26.98	17.70
F	2.63	3.43	2.33
Cl	0.34	0.75	0.36
Na	4.82	7.80	5.47
S	2.12	1.42	0.89
Ti	37.44	19.84	50.53

Table V Chemical Analysis of Sponge Titanium

Impurity*	Concentration (ppm by weight)	
	Sample 1	Sample 2
Si	1.7	1.0
O	59	20
Cl	24	18
K	45	37
Cr	4.4	4.7
Mn	23	26
Fe	6.8	7.9
Zn	5.3	7.2
As	1.1	1.7
Br	2.3	3.8
Rb	1.7	2.7

* Elements not listed may be present at a concentration level of < 1 ppm by weight.

Table VI Chemical Analysis for Arc-Melted Titanium Sponge

Impurity*	Concentration (ppm by weight)	
	Sample 1	Sample 2
Si	4.0	6.9
O	47	140
Cl	8.4	11.0
K	2.9	3.6
Cr	3.1	2.9
Mn	48	14.0
Fe	930	800
Zn	8.6	6.3
As	1.9	1.2
Br	3.0	1.8
Rb	2.6	1.4

* Elements not listed may be present at a concentration level of < 1 ppm by weight.

The Auger analysis was done in two steps. The first one determined the chemical constitution of the sample surface without sputtering. The next step was to sputter the surface with plasma bombardment to strip off the surface layer of the sample and supply the information on inner layers. Tables II and III are the Auger analysis results for sponge titanium and Table IV is the Auger analysis of arc-melted sponge titanium. For the arc-melted sponge titanium, we only did a Auger analysis without sputtering. The reason is that the volatile constituents are generally concentrated in the surface layers, the deeper the layer is detected, the less the amount of volatiles. This fact can be seen by comparing the data of Table II with the data of Table III.

Table II and IV indicate that each of the areas sampled have similar amounts of S, F, Na. The amount of C and O are different. The changes of the carbon and oxygen concentrations are believed to be caused by the contamination of the surrounding atmosphere in the arc-melting process. The amount of F and Cl change a little bit but it does not seems to be significant. From the Auger analysis, it is very difficult to decide which impurity

effects the TiNiSn crystal growth.

Comparing Table V with Table VI, one finds that the largest differences in the impurity concentrations are for Fe and Cl. The possible reasons for the increase in the Fe concentration in the arc-melting sample are contamination during the arc-melting process or by using tools to cut the sample. The reduction of Cl concentration is probably due to the volatile of $TiCl_3$ and/or $TiCl_4$ (boiling points 136 and 660 °C, respectively [11]).

Due to the failure of Fe, Cu, C, Cr and O, additions to change the phase of TiNiSn grown with crystal bar Ti, as well as the difference in the Cl content of the sponge titanium vs. the arc-melted sponge titanium and the crystal bar titanium, it was concluded that the Cl is the most likely factor affecting the crystal growth process and the resultant phase. In order not to introduce other factors which may affect the growth of TiNiSn, $NiCl_2$ was used as the controlling material. Amounts ranging from 33 ppm to 58 ppm weight of $NiCl_2$ (corresponding to from 10 to 18 ppm at.) were added to the starting materials. As the amount of $NiCl_2$ was increased, we observed a change in the resultant

phases from TiNiSn to Ni_3Sn_4 with a mixture of these two phases at intermediate concentrations. The experimental results clearly indicate the Cl is the key impurity in controlling the formation of Ni_3Sn_4.

The hypothesis of the effect of chlorine on the crystal growth may be thought of as follows. During the heating process, chlorine reacts with the titanium to form $TiCl_3$ and $TiCl_4$ which are quite volatile and condense out at the top of the quartz tube because the top of the crucible is cooler than its bottom. The Ti deposits on the wall of the quartz tube or the top of the crucible because of the disassociation of $TiCl_3$ and $TiCl_4$. The Cl_2 gas will diffuse back to the Ti surface and react with it to form $TiCl_3$ and $TiCl_4$ which then repeats the process. If there is sufficient time, or a large amount of Cl, there will be no titanium in the solution and thus few or no TiNiSn single crystals will be grown. Since the liquid contains only Ni and Sn, the Ni_3Sn_4 compound is formed.

Another possible explanation is that the presence of Cl prevents the nucleation of TiNiSn phase, and thus the Ni_3Sn_4 is formed instead.

X-ray diffraction confirmed that the flat phase is Ni_3Sn_4. To determine which explanation is correct, one needs further experimental proof and research.

CHAPTER IV

HEAT CAPACITY OF TiNiSn

A. Calorimeter

The vacuum calorimeter was introduced by Nernst for the measurement of specific heats at low temperature in the early 1900's. Its simplified form is showed in Figure 8, where the block B is a container, over which an insulated coil of platinum wire W is wound. B is suspended by the leads LL in a vacuum container C, which is cooled in a dewar D containing liquid helium. At the beginning, C is filled with helium gas at a low pressure, about 1 mm mercury, and the block B is cooled to the temperature of the bath by the heat transfer through the gas. After B has been cooled, the gas is pumped away after which B is thermally isolated. A known quantity of heat is applied to B by passing a known amount of current through the coil W for definite interval of time, and the resulting rise of temperature is measured by the change in resistance of the platinum wire. It is common now to have separate heaters and thermometers.

The vacuum in C prevents any heat transfer by gas

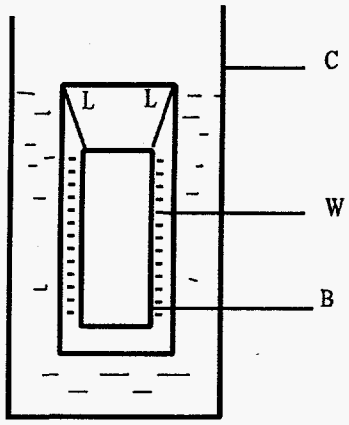

Figure 8. Schematic of a calorimeter

conduction or convection. At temperatures above 20 K, heat transfer by radiation , varying as T^4, become significant. This difficulty is overcome by adiabatic calorimetry as shown by Lange, Southard, and Andrews [12]. An adiabatic shield S (not shown) contains a separate heater, and is made to accurately follow the temperature of B. This is done by using a differential thermal couple between B and C. In order to avoid the absorbed helium gas, which spoils the vacuum of inside C, a polish metal plate having a good

thermal contact with C is made to press firmly against a similar polished metal disk attached to B (i.e. called a heat switch). This allows one to cool B down to the bath temperature. After the sample is cooled down the metal plate contacting B and C is removed, isolates B.

To measure of the heat capacity below 1.5 K one has to use ^{3}He as a coolant or use adiabatic demagnetization technique. The details of this technique are described by several articles in the references [13,14,15].

The cryostat which was used in this heat capacity measurement mainly consists of three parts - addenda, heat switch, thermal shield. The functions of addenda are to hold sample, heat it, and monitor the temperature change of sample. An electric heater and a resistance thermometer are connected with the addenda. The heat switch is used to cool the addenda and sample to the lowest possible temperature. A thermal shield made of seamless copper encloses the sample and the addenda. Its temperature can be controlled by a heater to maintain a temperature similar to the sample.

In the heat capacity measurement, the quantities measured are voltage drop of the thermal heater, the strength of the current passing through the heater, the

duration of heat pulse and the temperature change of the sample. The relationship between these quantities and the heat capacity can be expressed by the following equation:

$$C = \frac{\Delta Q}{\Delta T} = \frac{tV_H i}{(T_f - T_i)} = \frac{tV_H V_S}{R_S(T_f - T_i)} \qquad (11)$$

where

ΔQ - amount of heat absorbed

ΔT - temperature change

t - heating time

V_H - voltage drop of the heater

i - current passing through the heater

T_f - final temperature

T_i - initial temperature

V_S - voltage drop across a standard resistor

R_S - resistance of the standard resistor

In order to minimize the drift of the sample temperature, the temperature of the thermal shield was maintained to be equal to that of the sample. The recording and analysis of data was accomplished on a PC computer using the existing heat capacity analysis programs.

B. Experimental Results and Data Analysis

Generally the heat capacity at low temperature can be expressed by the equation:

$$C = \gamma T + \beta T^3 \qquad (12)$$

where γ is the coefficient of the linear term which represents the contribution of electrons to the heat capacity. The cubic term is the contribution from the lattice.

The curves for the heat capacity as function of temperature and the C/T vs. T^2 plot (inset) are given in Figure 9 . The measurement of heat capacity was carried out over the temperature range of 4.7 to 300 K. The γ value is obtained by extrapolating the C/T vs T^2 data to 0 K.

The γ value obtained in our experiment was -0.2(±0.4) mJ/mol K^2 (see inset of Figure 9). Since γ cannot be a negative number, and since the uncertainty is twice as large as the intercept (γ), |0.4| vs. |0.2|, γ can be considered to essentially zero. The reported γ values are 0.7 (±0.3) [5 and 16] and 0.9 [7] mJ/mol K^2. The difference between our value and the reported ones is that our heat capacity data only go down to ~5 K, while those of Aliev and co-

workers [5 and 16] and Kuentzler et al. [7] go down to ~1.5 K, and since γ is obtained by extrapolation to T = 0 K, the literature values are probably more likely to be correct. Indeed, a close examination of the data shown in the inset of Figure 9 indicates that there is a slight upward curvature for the lowest data points, and using only the three lowest temperature data points a γ value of ~0.4 mJ/mol K^2 is obtained, which is in fair agreement with literature.

The β coefficient of the cubic term in equation (11) is related to the Debye temperature (Θ_D) by the equation $\Theta_D=(12\pi^4Rn/5\beta)^{1/3}$, where R is the gas constant and n is the number of atoms in the formula unit (n=3 for TiNiSn). The β value obtained in our experiment is 0.0527 (±0.0070) mJ/mol K^4 and this gives a value of 335 (±15) K for the Debye temperature. This value falls between the value reported by Aliev [5 and 16], 283 K, and the value calculated from the C/T vs T^2 graph presented by Kuentzler et al. [7], 409 K. These results suggest that the low temperature properties of TiNiSn are quite sensitive to the chemical composition (i.e., the variation of the ratios of the three components from 1:1:1 of the ideal composition) and/or impurities.

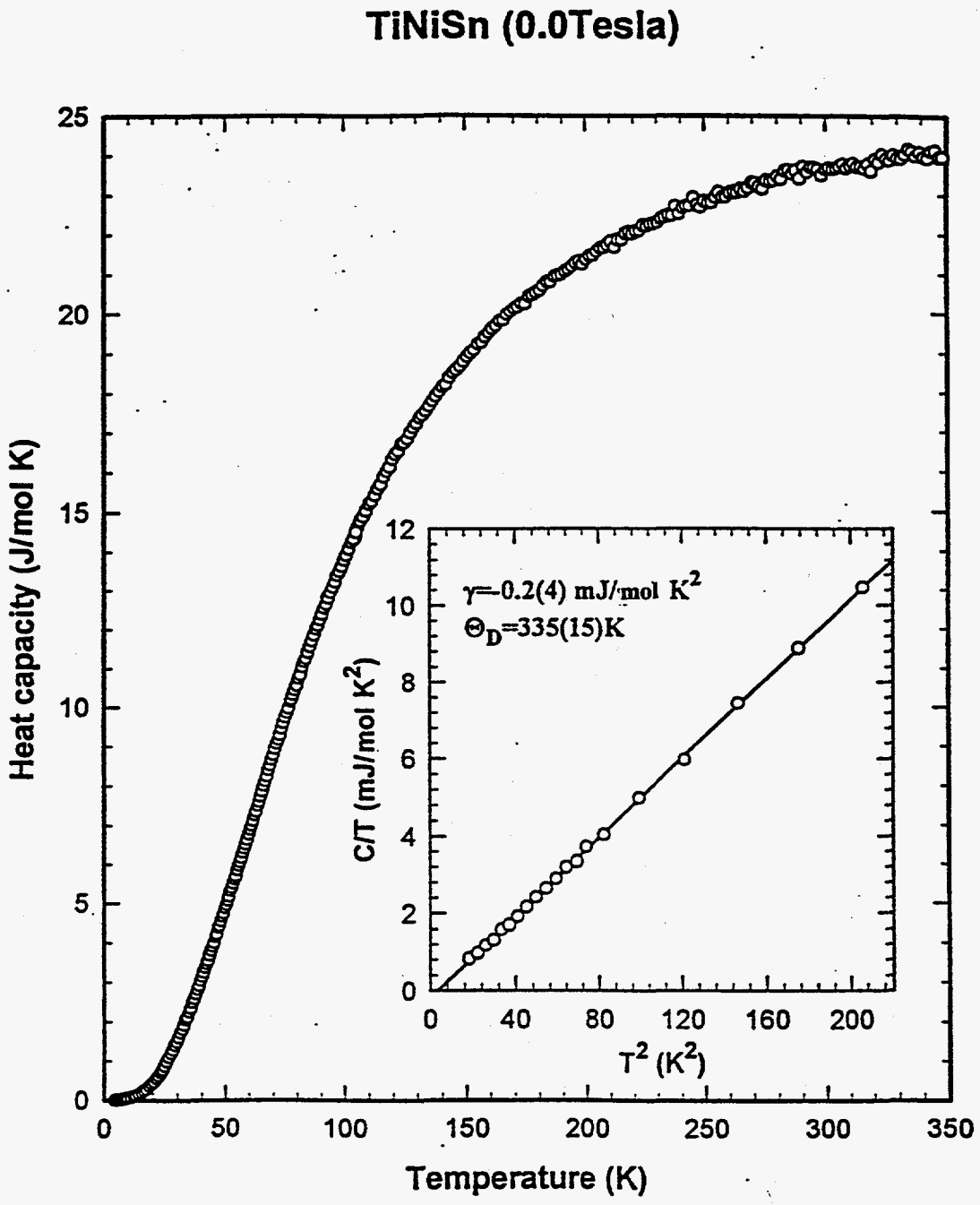

Figure 9. Heat Capacity curves of TiNiSn.

CHAPTER V

SUSCEPTIBILITY OF TiNiSn

A. Susceptometer

Macroscopically, the magnetism of solids is described by a susceptibility. For the crystal materials with cubic symmetry or homogeneous non-cubic materials, their magnetization

$$M = \chi H \qquad (13)$$

$$\chi = \frac{M}{\mathrm{H}} = \frac{\mu_0 M}{B_0} \qquad (14)$$

where

χ - the magnetic susceptibility

M - magnetization

H - the strength of the magnetic field.

μ_0 - permeability of vacuum ($4\pi \times 10^{-7}$ Hm^{-1})

B - magnetic flux density

According to the sign and the value of the susceptibility, the magnetic property of a solid can be

classified into diamagnetism, paramagnetism, ferromagnetism and ferrimagnetism and antiferromagnetism. By investigating the susceptibility of a materials, we can better understand its nature. An explanation of the magnetic properties for solid materials can be found in most text books on solid state physics.

Susceptibility can be measured by a Faraday balance or a SQUID susceptometer. The former measures the weight change of a sample with or without an applied magnetic field. The latter measures the change of mutual induction. When a magnetic material is moving in a magnetic field, it will affect the distribution of the magnetic field lines. When a sample moves within the space of a wire coil, its movement will change the flux density of the magnetic field, therefore change the induction of a second coil. By sensing this change, the susceptibility can be detected. The design of a susceptometer can be found in the reference [17].

In the measurement of the susceptibility, we used a SQUID. The schematic of the susceptometer is shown in Figure 10. It consists of three essential elements:

1. A source of uniform DC magnetic field.
2. A system of pickup coils within which the

sample is moved.

3. A SQUID sensor which measures the current in the pickup coil.

B. Experimental Results and Data Analysis

The susceptibility measurement is done on a SQUID susceptometer with a maximum DC magnetic field of 55,000 gauss. In our measurements of the susceptibility of TiNiSn, a DC magnetic field 10,000 gauss was used. The curves of susceptibility versus temperature is given in Figure 11.

This measurement indicates that the magnetic susceptibility of TiNiSn is very small. In the low temperature range there is a small tail. It might result from the background of the disk which holds the sample and/or the impurities in the sample. Glue refers to the peak around 50 K. It is magnetic ordering in thin films of oxygen (melting point 54.75 K). Our data give a positive values over all temperature range, which indicates TiNiSn a weakly paramagnetic material. The low values for the paramagnetic susceptibility of TiNiSn is consistent with the low electronic specific heat constant obtained from the heat capacity measurements.

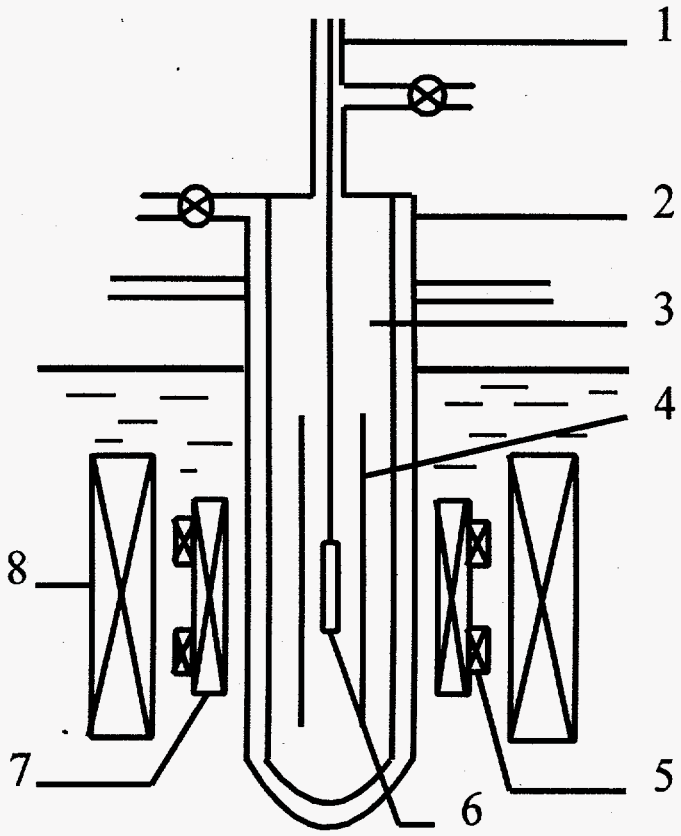

Figure 10. Schematic of a susceptometer. 1.Assembly for introducing sample. 2. Double walled glass tube. 3. Sample space. 4. Coil-foil tube. 5. Secondary coil. 6. Sample and sample holder. 7. Primary coil. 8. Superconducting magnet.

Stadnyk and Skolozdra [6] measured the susceptibility of TiNiSn from 78 K to 300 K. They concluded that TiNiSn was a paramagnetic material.

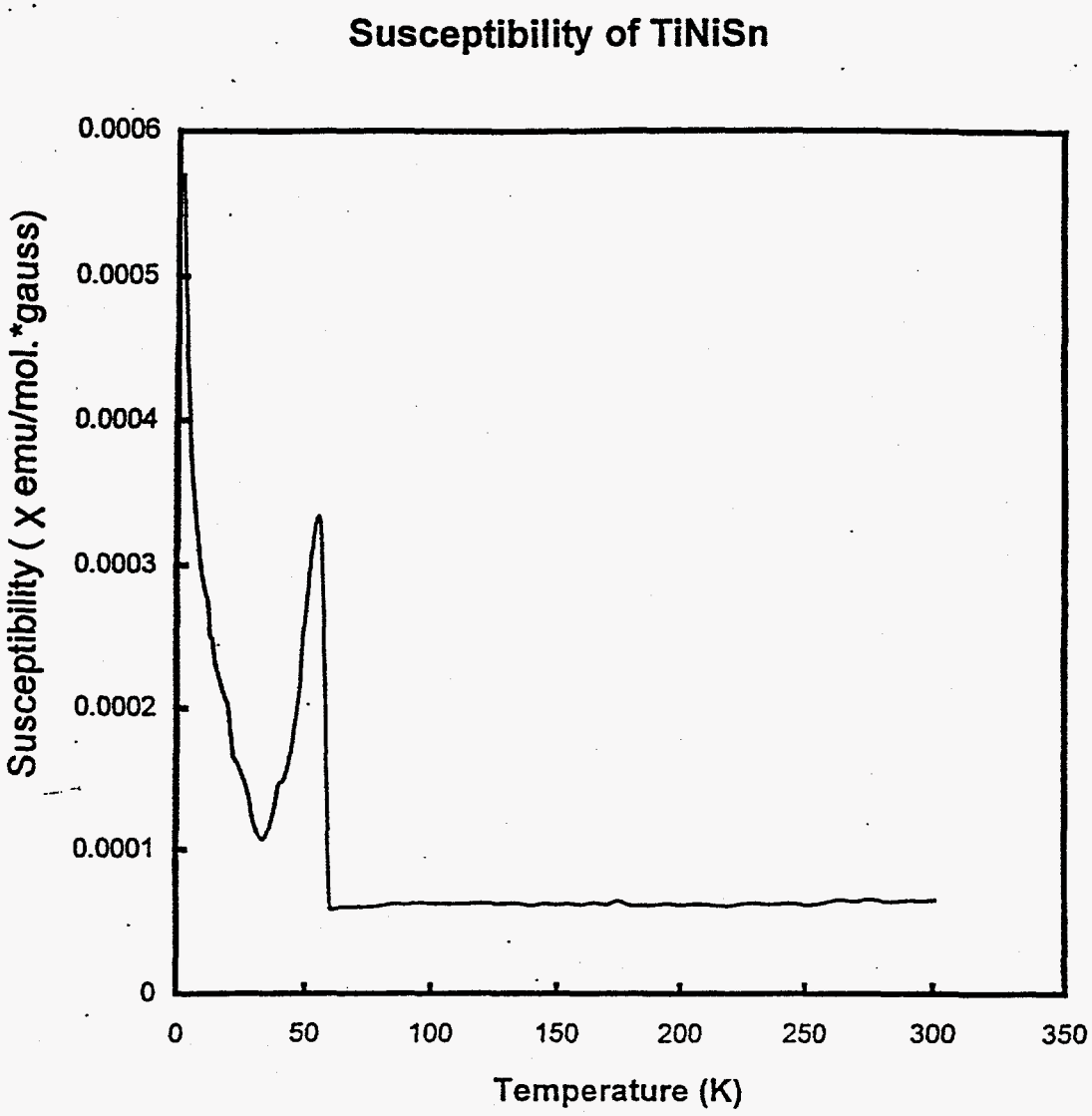

Figure 11. Susceptibility of TiNiSn.

CHAPTER VI

CONCLUSION AND SUMMARY

1. The TiNiSn single crystals were successfully grown by a flux growth method with the temperature range from 600 - 1120 °C. Sn was chosen to be the flux material. The elemental atom ratio used in this study is 9:9:91(Ti:Ni:Sn). P. C. Canfield and Z. Fisk had used this method growing a series crystals including TiNiSn in 1992 [9].

2. Chlorine, which was an impurity in the titanium sponge starting material, has a big effect on the resultant crystal phase. When the chlorine concentration is too high (> 100 ppm at.) the TiNiSn phase can not be grown, instead one obtains crystals of Ni_3Sn_4. Two possible explanations are proposed for this observation.

High chlorine contents lead to the removal of titanium from the flux by vapor transport via $TiCl_3$ and $TiCl_4$ to the cold portions of the growth container, as a result there is not enough titanium to form TiNiSn;

Chlorine can prevent the nucleation of TiNiSn. When the concentration of chlorine is beyond a certain limit, no

TiNiSn crystal can be grown.

3. The chlorine concentration in the titanium sponge can be lowered by preheating the titanium sponge at a temperature over 700 °C in a high vacuum or by arc melting. Crystal bar titanium is a better choice for growing titanium compounds, since it has a low chlorine content.

4. Both TiNiSn and PtMnSb have a fcc MgAgAs structure. Their lattice parameters are 5.931Å and 6.199Å, respectively.

5. Heat capacity measurement of TiNiSn indicates there is no magnetic order in TiNiSn. The electron specific heat constant and Debye temperature were found to be ~0 mJ/mol·K^2 and 335 K, respectively.

6. The magnetic susceptibility measurement indicated that the TiNiSn is a weak paramagnetic material with a susceptibility value about 10^{-5} emu/mol.*gauss around room temperature.

REFERENCES

1. R. A. de Groot, F. Muller, P. G. van Engen and K. H. J. Buschow, Phys. Rev. Lett. 50 (1983) 2024.

2. K. E. H. Hanssen and P. E. Mijnarends, Phys. Rev. B34 (1986) 5009.

3. K. H. J. Buschow, P. G. Van Engen and R. Jongebreur. J. Magn. and Magn. Mater., 38 (1983)1-22.

4. F. G. Aliev, N. B. Brandt, V. V. Moshchalkov, R.V. Skolozdra, and A. I. Belogrokhov. Z. Physics B-Condensed Matter. 75, 167-171 (1989).

5. F. G. Aliev, V. V. Kozyrkov, V. V. Moshhchalkov, R. V. Scolozdra, and K. Durczewski. Z. Physik B - Condensed Matter. 80, 333-357 (1990)

6. R. V. Skolozdra, Yu. V. Stannnyk, E. E. Starodynova, (L'vov. Gos. Univ., Lovv, USSR). Ukr. Fiz. zh. 1986, 31(8), 1258-61 (Russ); abstracted in Chem. Abstr. 105, 202172e, 1987.

7. R. Kuentzler, R. Clad, G. Schmerber and Y. Dossmann. J. Magn. Magn. Mater. 104-107 (1992) 1976-1978.

8. W. Keitschko. Metallurgical Transactions, Volume 1, November 1970, 3159-3162.

9. P. C. Canfield and Z Fisk, Philosophical Magazine, B65,

1117-1123 (1992).

10. B. D. Cullity, Elements of X-ray Diffraction, 2nd Edition, Addison-Wesley Publishing Company, Inc., 1978.
11. CRC Handbook of Chemistry and Physics, David R. Lide Edition-Chief, 4-92, 76th Edition, 1995-1996.
12. Z.F. Lange, Phys. Chem., 110,343(1924). J. Franklin Inst., J. C. Southard and D. H. Andrews, 209, 349 (1930).
13. Experimental Techniques in Low Temperature Physics, G. K. White, Clarendon, Oxford, 1959.
14. Experimental Cryophysics, F. E. Hoare, L. C. Jackson, and N. Kurti, Butterworth, London, 1961.
15. Low temperature Techniques, F. Din and A. H. Cocken, Newnes, London, 1960.
16. F. G. Aliev, Physica B 171 (1991)199-205.
17. Magnetic Susceptibility of Superconductors and Other Spin Systems. Robert A. Hein, Thomas L. Francavilla and Donald H. Liebenberg. 1991 Plenum Press, New York.

ACKNOWLEDGEMENTS

After a long time, this thesis is at last finished. I would like to express my sincere thanks to Dr. Karl Gschneidner Jr. and Dr. Paul Canfield. Without their careful guidance I would not have been able to finish this thesis. Their broad knowledge and serious attitude of research will be forever kept in my memory.

I would like also thank to Dr. Paul Canfield who helped me to do the susceptibility measurements . Thanks to Dr. Vitali Pecharsky for his work on the heat capacity measurement. I also thank to Ms. Tamy Blooner and Cheryl (Bradley) Kamman for their assistance in the analysis of elements.

APPENDIX

Experiment Data for the Susceptibility Measurement of TiNiSn

Temperature (K)	χ (emu/mol*gauss)	Temperature (K)	χ (emu/mol*gauss)
1.998	0.00057	48.013	0.000214
2.499	0.00053	50.012	0.000264
3.004	0.000495	56.02	0.000326
3.5	0.000464	60.001	5.99 E-5
4.008	0.000439	63.995	6.05E-5
5.003	0.000396	69.992	6.06E-5
5.999	0.000364	75.987	6.06E-5
7.009	0.000341	79.988	6.13E-5
8.001	0.00032	85.989	6.31E-5
9.006	0.000305	89.985	6.24E-5
10.007	0.000293	95.977	6.37E-5
11.009	0.000282	99.969	6.32E-5
12.006	0.000276	104.97	6.29E-5
13.007	0.000251	109.97	6.28E-5
14.006	0.000249	114.96	6.28E-5
15.017	0.000233	119.95	6.32E-5
16.016	0.000225	124.95	6.31E-5
17.016	0.000218	129.94	6.3E-5
18.016	0.000212	134.94	6.33E-5
19.016	0.000206	139.93	6.15E-5
20.016	0.000201	144.93	6.31E-5
22.021	0.000168	149.93	6.22E-5
24.021	0.00016	154.93	6.3E-5
26.02	0.000151	159.93	6.19E-5
28.021	0.000139	164.92	6.35E-5
30.02	0.000118	169.92	6.21E-5
32.02	0.00011	174.92	6.48E-5
34.02	0.000107	179.92	6.17E-5
36.019	0.000114	184.92	6.16E-5
38.019	0.000128	189.92	6.19E-5
40.019	0.000146	194.91	6.29E-5
41.812	0.000149	199.9	6.18E-5
44.013	0.000163	204.88	6.25E-5
46.01	0.000188	209.89	6.23E-5

Temperature (K)	χ (emu/mol*gauss)	Temperature (K)	χ (emu/mol*gauss)
214.88	6.13E-5	259.89	6.4E-5
219.88	6.13E-5	264.9	6.53E-5
224.88	6.26E-5	269.92	6.4E-5
229.88	6.34E-5	274.91	6.59E-5
234.88	6.23E-5	280.6	6.44E-5
239.88	6.27E-5	284.92	6.41E-5
244.88	6.32E-5	290.6	6.52E-5
249.88	6.17E-5	295.61	6.47E-5
254.89	6.22E-5	300.64	6.53E-5